APPENDICES – WAVES AND PATTERNING IN DEVELOPMENTAL BIOLOGY: VERTEBRATE SEGMENTATION AND FEATHER BUD FORMATION AS CASE STUDIES

RUTH E. BAKER, SANTIAGO SCHNELL AND PHILIP K. MAINI

ABSTRACT. In this article we will discuss the integration of developmental patterning mechanisms with waves of competency, which control the ability of a homogeneous field of cells to react to pattern forming cues and generate spatially heterogeneous patterns. We base our discussion around two well known patterning events which take place in the early embryo: somitogenesis and feather bud formation. We outline mathematical models to describe each patterning mechanism, present the results of numerical simulations and discuss the validity of each model in relation to our example patterning processes.

APPENDIX A. CLOCK AND WAVEFRONT MODEL

In (Baker et al., 2006a,b) we develop a mathematical formulation of the clock and wavefront model using the assumptions of Pourquié and co-workers: the segmentation clock controls *when* the boundaries of the somites form and the FGF8 wavefront controls *where* they form (Dubrulle et al., 2001; Tabin and Johnson, 2001; Dubrulle and Pourquie, 2002). In addition, we assume the following: (i) once cells reach the threshold level of FGF8, they become competent to segment by gaining the ability to respond to a chemical signal, thereby producing a somitic factor; (ii) after reaching the threshold level, cells undergo one oscillation of the segmentation clock and then become competent to produce the aforementioned signal; (iii) once a cell reacts to the signal and becomes part of a somite, it becomes refractory to FGF signalling. A cell becomes part of a coherent somite with other cells which begin to produce a high level of somitic factor at a similar time.

The mathematical model is based around the signalling model for somitogenesis, first proposed by Maini and co-workers (Collier et al., 2000; Baker et al., 2003; McInerney et al., 2004; Schnell et al., 2002). A verbal description of the model (first proposed in (Primmett et al., 1989)) can be outlined as follows: at a certain time, a small fraction of cells at the anterior-most end of the PSM will have undergone a whole oscillation of the segmentation clock after reaching the determination front. These *pioneer cells* will produce and emit a signal which will diffuse along the PSM. Any cell which has a level of FGF8 below that expressed at the determination front will respond to the signal by producing a somitic factor. At this point, a cell is specified as somitic and it will go on to form a somite during subsequent oscillations of the segmentation clock: groups of cells which begin producing somitic factor concurrently will form part of a somite together. The process begins once again when cells now at the anterior end of the PSM become competent to signal. A negative feedback loop between somitic factor and signalling molecule results in periodic pulses in the signal and hence the specification of somites at regular time intervals.

The mathematical model constructed from Pourquié's descriptive clock and wavefront model consists of a coupled system of three non-linear PDEs. The variables which the system describes are a *somitic factor* which determines the fate of cells (cells can only form part of a somite with a high level of somitic factor), a *diffusive signalling molecule* produced by the pioneer cells at the anterior-most end of the PSM and FGF8, which is able to confer the ability upon cells to produce somitic factor and signalling molecule (according to their level of expression of FGF8).

We choose to model the gradient by assuming that FGF8 is produced only in the tail, that it diffuses out from the tail along the PSM and undergoes linear decay (see (Baker et al., 2006b) for more details). The FGF8 gradient moves in a posterior direction along the PSM and confers the ability upon cells to produce a somitic factor; at time t_s later they gain the ability to signal. Somitic factor production is activated in response to a pulse in signalling molecule emitted from the pioneer cells at the anterior end of the PSM. Rapid inhibition of signal production by the somitic factor ensures that peaks in signal concentration are transient and produced at regular intervals (see (McInerney et al., 2004) for further details).

The system of non-linear PDEs describes the dynamics of somitic factor (u) signalling molecule (v) and FGF8 (w) and can be written as follows (Baker et al., 2006a,b):

$$\frac{\partial u}{\partial t} = \frac{(u+\mu v)^2}{\gamma+u^2}\chi_u - u, \tag{1}$$

$$\frac{\partial v}{\partial t} = \kappa\left(\frac{\chi_v}{\epsilon+u} - v\right) + D_v\frac{\partial^2 v}{\partial x^2}, \tag{2}$$

$$\frac{\partial w}{\partial t} = \chi_w - \eta w + D_w\frac{\partial^2 w}{\partial x^2}, \tag{3}$$

where μ, γ, κ, ϵ, η, D_v, D_w are positive parameters. Production of u, v and w are controlled by the respective Heaviside functions[1]

$$\chi_u = H(w^* - w), \tag{4}$$

$$\chi_v = H(t - t^*(w^*, x) - t_s), \tag{5}$$

$$\chi_w = H(x - x_n - c_n t), \tag{6}$$

where w^* is the level of FGF8 at the determination front, $t^*(w^*, x)$ is the time at which a cell at x reaches the determination front (*i.e.* $w(x, t^*) = w^*$), t_s is the period of the segmentation clock, x_n represents the initial position of the tail and c_n represents the rate at which the AP axis is extending.

Somitic factor production is activated by the signal and is self-regulating. High levels of somitic factor also inhibits production of the signal, which is able to diffuse. For a more detailed explanation of the system of equations describing the somitic factor and the signal see (Collier et al., 2000; Schnell et al., 2002; McInerney et al., 2004). FGF8 is produced only in the tail region of the embryo.

The boundary conditions are taken to be

$$\begin{array}{l} u, v \to 0 \quad \text{as} \quad x - \{x_n + ct\} \to +\infty, \\ u, v \quad \text{are bounded as} \quad x - \{x_n + ct\} \to -\infty, \\ w \quad \text{is bounded as} \quad x - \{x_n + ct\} \to +\infty, \\ w \to 0 \quad \text{as} \quad x - \{x_n + ct\} \to -\infty. \end{array} \tag{7}$$

The initial conditions for u and v are taken to be (McInerney et al., 2004):

$$u(x, 0) = \begin{cases} 1 & \text{if } x \le 0, \\ 0 & \text{if } x > 0, \end{cases} \tag{8}$$

and

$$v(x, 0) = A^* H(-x) + B^* \cosh(\lambda(l - |x|)), \tag{9}$$

where

$$A^* = \frac{1}{1+\epsilon-\epsilon_1}, \qquad B^* = \frac{A^* \text{sign}(x)}{2\cosh(\lambda l)}, \qquad \lambda = \sqrt{\frac{\kappa}{D_v}}, \tag{10}$$

[1]The Heaviside function $H(x)$ is equal to unity if $x > 0$ and zero otherwise: in this way it acts like a switch.

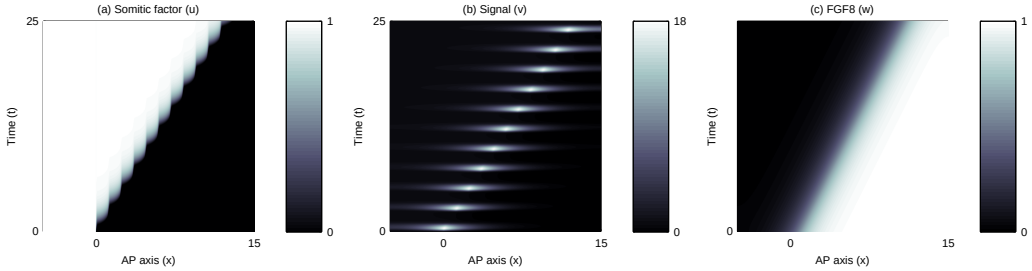

Figure 1. Numerical solution of the clock and wavefront model in one spatial dimension. Continuous regression of the FGF8 wavefront (c), is accompanied by a series of pulses in signalling molecule (b), and coherent rises in somitic factor concentration (a).

and $\epsilon_1 \ll 1$. Since w evolves to a travelling wave profile (Baker, 2005; Baker et al., 2006b):

$$w_{tw}(x) = \begin{cases} \frac{n_-}{\eta(n_- - n_+)} \exp\{n_+(x - x_n - c_n t)\} & \text{if} \quad x - x_n - c_n t \leq 0, \\ \frac{n_+}{\eta(n_- - n_+)} \exp\{n_-(x - x_n - c_n t)\} + \frac{1}{\eta} & \text{if} \quad x - x_n - c_n t > 0, \end{cases} \tag{11}$$

we take the initial condition for w to be the state of the travelling wave at time $t = 0$.

We solved the mathematical formulation of the model numerically using the NAG library routine D03PCF and the results were plotted using the MATLAB function imagesc. Figures 1(a)–(c) shows the dynamics of somitic factor, signalling molecule and FGF8, respectively. We see that the region of high FGF8 expression moves in a posterior direction along the AP axis with constant speed. A sequence of successive signals, moving in a posterior direction, produces a series of coherent rises in the level of somitic factor which then enables cells to progress to form discrete somites.

APPENDIX B. REACTION-DIFFUSION MODEL

We consider two chemicals: an activator (u) and an inhibitor (v). The interactions between u and v and their movement through space can be modelled by the following system of PDEs (Turing, 1952):

$$\frac{\partial u}{\partial t} = \nabla.(\nabla u) + f(u, v), \tag{12}$$

$$\frac{\partial v}{\partial t} = \nabla.(D\nabla v) + g(u, v), \tag{13}$$

where $\boldsymbol{x} \in \mathcal{D}$ and $t \in [0, \infty)$. The left-hand side of each equation represents the change in chemical concentration over time, the first terms on each of the right-hand sides represent diffusion of the chemical throughout the volume under consideration and the second terms the interactions between the chemicals.

Assuming that there is no loss of chemical through the boundary of the domain, we have zero flux boundary conditions of the form $\boldsymbol{n}.\nabla u = 0 = \boldsymbol{n}.\nabla v$ for $\boldsymbol{x} \in \partial\mathcal{D}$ where $\boldsymbol{n}$ is the unit normal to the boundary $\partial\mathcal{D}$. Working in one spatial dimension, the domain is given by $x \in \mathcal{D} = (0, L)$ and the boundary conditions can be written as $\partial u/\partial x = 0 = \partial v/\partial x$ for $x = 0, L$.

The condition for *diffusion-driven instability* (Turing, 1952), and hence a spatial pattern in chemical concentration, is that the steady state concentrations of u and v must be stable to small perturbations in the absence of diffusion, but become unstable when diffusive effects are added.

We demonstrate this phenomenon with an example using the Gierer-Meinhardt scheme (Gierer and Meinhardt, 1972) to describe the interactions between u and v:

$$\frac{\partial u}{\partial t} = \nabla.(\nabla u) + \frac{u^2}{v} - bu, \tag{14}$$

$$\frac{\partial v}{\partial t} = \nabla.(D\nabla v) + u^2 - v, \tag{15}$$

where $b > 0$. Here u activates its own production (self-activation) and also that of v, whilst v inhibits both its own production (self-inhibition) and that of u. The spatially uniform steady states (u_0, v_0) of the model satisfy

$$\frac{u_0^2}{v_0} - bu_0 = 0 = u_0^2 - v_0 \quad \Rightarrow \quad (u_0, v_0) = \left(\frac{1}{b}, \frac{1}{b^2}\right). \tag{16}$$

We wish to investigate the stability of this steady state to small perturbations in u and v concentration. Letting $u = u_0 + \tilde{u}$ and $v = v_0 + \tilde{v}$, where $\tilde{u}$ and $\tilde{v}$ are small, and substituting into equations (14), (15) gives

$$\frac{\partial \tilde{u}}{\partial t} = \nabla.(\nabla \tilde{u}) + \frac{(u_0 + \tilde{u})^2}{(v_0 + \tilde{v})} - b(u_0 + \tilde{u}), \tag{17}$$

$$\frac{\partial \tilde{v}}{\partial t} = \nabla.(D\nabla \tilde{v}) + (u_0 + \tilde{u})^2 - (v_0 + \tilde{v}). \tag{18}$$

Considering only terms which are linear in $\tilde{u}$ and $\tilde{v}$ we have the following system

$$\frac{\partial \tilde{u}}{\partial t} = \nabla.(\nabla \tilde{u}) + b\tilde{u} - b^2\tilde{v}, \tag{19}$$

$$\frac{\partial \tilde{v}}{\partial t} = \nabla.(D\nabla \tilde{v}) + \frac{2}{b}\tilde{u} - \tilde{v}, \tag{20}$$

which describes the behaviour whilst $|\tilde{u}|, |\tilde{v}|$ remain small. To see if small perturbations to the system will grow, we consider finding solutions for $\tilde{u}$ and $\tilde{v}$ which are of the form

$$\tilde{u} = \alpha \exp(\lambda t + ik\boldsymbol{x}), \quad \tilde{v} = \beta \exp(\lambda t + ik\boldsymbol{x}). \tag{21}$$

The term $\exp(ik\boldsymbol{x})$ describes the spatial pattern, whilst the term $\exp(\lambda t)$ describes the amplitude of the spatial oscillations. For a stable steady state, small disturbances must decay with time and hence the real part of λ must be negative, whilst for fluctuations to grow into a spatial pattern the real part of λ must be positive.

Substituting (21) into equations (19) and (20) gives

$$\begin{pmatrix} \lambda\tilde{u} \\ \lambda\tilde{v} \end{pmatrix} = \begin{pmatrix} b - k^2 & -b^2 \\ 2/b & -1 - Dk^2 \end{pmatrix} \begin{pmatrix} \tilde{u} \\ \tilde{v} \end{pmatrix}, \tag{22}$$

which has solutions if and only if

$$\lambda^2 + [(D+1)k^2 + (1-b)]\lambda + h(k^2) = 0, \tag{23}$$

where

$$h(k^2) = Dk^4 + (1 - bD)k^2 + b. \tag{24}$$

For the steady state to be stable in the absence of diffusion ($k^2 = 0$) the solutions of

$$\lambda^2 + (1-b)\lambda + b = 0, \tag{25}$$

must have negative real parts. This occurs if $b < 1$. For the steady state to be unstable in the presence of diffusion ($k^2 \neq 0$) equation (23) must have at least one root with positive real part. Since $b < 1$, this occurs if $h(k^2) < 0$ for some $k^2 \neq 0$. The minimum of $h(k^2)$ occurs where

$$\frac{dh(k^2)}{dk^2} = 2Dk^2 + (1 - bD) = 0 \quad \Rightarrow \quad k^2_{crit} = \frac{Db - 1}{2D}, \tag{26}$$

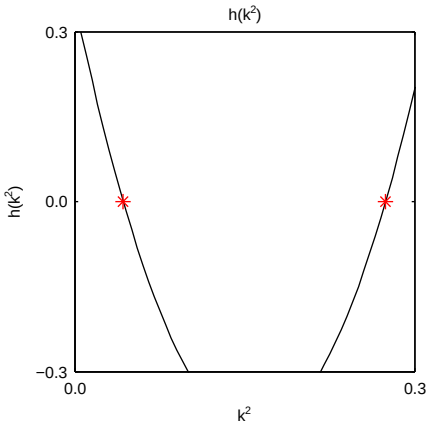

Figure 2. A plot of $h(k^2)$ as given by equation (24). The roots are given approximately by $k_-^2 = 0.0426$ and $k_+^2 = 0.2741$ (red asterisks), which gives a range of admissible modes: $n = 6, 7, \ldots, 13$. Parameters are as follows: $D = 30$ and $b = 0.35$.

and hence we see that $h(k^2) < 0$ if $Db > 3 + 2\sqrt{2}$. The wave numbers of the admissible modes, *i.e.* the values of k^2 which result in a spatially heterogeneous solution, are those such that $k_-^2 < k^2 < k_+^2$ where

$$k_\pm^2 = \frac{1}{2D}\left[(bD-1) \pm \sqrt{(bD-1)^2 - 4Db}\right]. \tag{27}$$

The general solution of the linearised sytem (in 1D) can be written in the form

$$\tilde{u}(x,t) = e^{\lambda(k^2)t}\left[A\cos(kx) + B\sin(kx)\right], \tag{28}$$

$$\tilde{v}(x,t) = e^{\lambda(k^2)t}\left[\tilde{A}\cos(kx) + \tilde{B}\sin(kx)\right]. \tag{29}$$

The boundary condition at $x = 0$ gives $B, \tilde{B} = 0$ whilst the boundary condition at $x = L$ requires that for a non-trivial solution $kL = n\pi$ for $n = 0, 1, 2, \ldots$ The general solution can now be written as a combination of the admissible modes:

$$\tilde{u}(x,t) = \sum_n A_n e^{\lambda(k^2)t}\cos\left(\frac{n\pi x}{L}\right) \quad \text{and} \quad \tilde{v}(x,t) = \sum_n \tilde{A}_n e^{\lambda(k^2)t}\cos\left(\frac{n\pi x}{L}\right), \tag{30}$$

where the n satisfy

$$k_-^2 < \left(\frac{n\pi x}{L}\right)^2 < k_+^2. \tag{31}$$

Figure 4 (main text) shows the results of numerical solution of the system in one spatial dimension using the MATLAB function pdepe. The field is initially at the homogeneous steady state, with small random fluctuations added to u. Over time, the fluctuations are amplified into a series of peaks and troughs in chemical concentration, with mode $n = 9$ chosen in this particular simulation: this is consistent with the set of admissible modes given in Figure 2. Parameters are as follows: $D = 30$ and $b = 0.35$. By way of illustration of the different patterning possibilities, Figure 5 (main text) shows numerical simulation of the system in two spatial dimensions using the same parameter values, carried out using COMSOL MULTIPHYSICS.

Notice that with the GM kinetics, the pattern of peaks and troughs coincide as the kinetics are of *pure* activator-inhibitor type: the Jacobian matrix, $\mathcal{J}$, describing the interactions between u and

v is of the form

$$\mathcal{J} = \begin{pmatrix} \frac{\partial f}{\partial u} & \frac{\partial f}{\partial v} \\ \frac{\partial g}{\partial u} & \frac{\partial g}{\partial v} \end{pmatrix} = \begin{pmatrix} + & - \\ + & - \end{pmatrix}. \tag{32}$$

However, the Schakenberg kinetics (Schnakenberg, 1979), for example, are of *cross* activator-inhibitor type:

$$\mathcal{J} = \begin{pmatrix} \frac{\partial f}{\partial u} & \frac{\partial f}{\partial v} \\ \frac{\partial g}{\partial u} & \frac{\partial g}{\partial v} \end{pmatrix} = \begin{pmatrix} + & + \\ - & - \end{pmatrix}, \tag{33}$$

and in this case, a peak in u concentration coincides with a trough in v concentration.

APPENDIX C. CELL-CHEMOTAXIS MODEL

We consider cell density (n) and activator concentration (c). The interactions between cells and the chemical and their movement through space can be modelled by the following system of PDEs (Murray, 2003):

$$\frac{\partial n}{\partial t} = \nabla.(D\nabla n) - \nabla.(\chi(c)n\nabla c) + f(n,c), \tag{34}$$

$$\frac{\partial c}{\partial t} = \nabla.(\nabla c) + g(n,c), \tag{35}$$

where $\boldsymbol{x} \in \mathcal{D}$ and $t \in [0,\infty)$. The first term on the RHS of each equation represents the random motion/diffusion of cells/chemical. The second term in the equation describing cell density represents the chemotaxis term, with cells moving up gradients in chemical concentration if $\chi(c) > 0$. The remaining terms on the RHS represent cell (chemical) proliferation (production) and decay.

Assuming that there is no loss of cells or chemical through the boundary of the domain, we have zero flux boundary conditions of the form $\boldsymbol{n}.\nabla n = 0 = \boldsymbol{n}.\nabla c$ for $\boldsymbol{x} \in \partial\mathcal{D}$, where $\boldsymbol{n}$ is the unit normal to the boundary, $\partial\mathcal{D}$. Working in one spatial dimension, the domain is given by $x \in (0, L)$ and the boundary conditions can be written as $\partial n/\partial x = 0 = \partial c/\partial x$ for $x = 0, L$.

In this case, we require that the steady states of cell density and chemical concentration are unstable when diffusive and chemotactic effects are present. We demonstrate this phenomenon using the following scheme (Myerscough et al., 1990, 1998):

$$\frac{\partial n}{\partial t} = \nabla.(D\nabla n) - \nabla.(\chi n\nabla c) + rn(N-n), \tag{36}$$

$$\frac{\partial c}{\partial t} = \nabla.(\nabla c) + \frac{n}{1+n} - c, \tag{37}$$

where D, χ, r and N are all positive parameters. Here cell density controls chemical production, with saturation for high cell density, and the chemical undergoes linear decay. Cell proliferation is controlled via a logistic growth term, with carrying capacity N. The spatially uniform steady states (n_0, c_0) of the model are given by

$$n_0 = N \quad \text{and} \quad c_0 = \frac{N}{1+N}. \tag{38}$$

We wish to investigate the stability of this steady state to small perturbations in cell density and chemical concentration. Letting $n = n_0 + \tilde{n}$ and $c = c_0 + \tilde{c}$, where $\tilde{n}$ and $\tilde{c}$ are small, and substituting into equations (36) and (37) gives

$$\frac{\partial \tilde{n}}{\partial t} = \nabla.(D\nabla\tilde{n}) - \nabla.[\chi(n_0+\tilde{n})\nabla\tilde{n}] - r\tilde{n}(N+\tilde{n}), \tag{39}$$

$$\frac{\partial \tilde{c}}{\partial t} = \nabla^2\tilde{c} + \frac{(N+\tilde{n})}{1+(N+\tilde{n})} - \left(\frac{N}{1+N} + \tilde{n}\right). \tag{40}$$

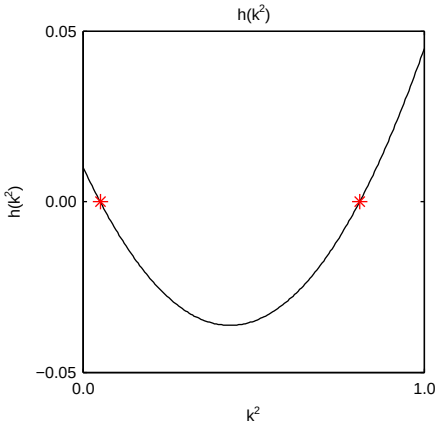

Figure 3. A plot of $h(k^2)$ given by equation (45). The roots are given approximately by $k_-^2 = 0.0493$ and $k_+^2 = 0.8107$ (red asterisks), which gives a range of admissible modes: $n = 6, 7, \ldots, 22$. Parameters are as follows: $D = 0.25$, $\chi = 1.9$, $r = 0.01$ and $N = 1.0$.

Considering only terms which are linear in $\tilde{n}$ and $\tilde{c}$ we have the following system:

$$\frac{\partial \tilde{n}}{\partial t} = D\nabla^2\tilde{n} - \chi N\nabla^2\tilde{n} - rN\tilde{n}, \tag{41}$$

$$\frac{\partial \tilde{c}}{\partial t} = \nabla^2\tilde{c} + \frac{N\tilde{n}}{(1+N)^2} - \tilde{c}, \tag{42}$$

which describes the behaviour whilst $|\tilde{n}|, |\tilde{c}|$ remain small. To see if small perturbations to the system will grow, we consider finding solutions for $\tilde{n}$ and $\tilde{c}$ which are of the form $\tilde{n} = \alpha\exp(\lambda t + ik\boldsymbol{x})$ and $\tilde{c} = \beta\exp(\lambda t + ik\boldsymbol{x})$. To ensure that small fluctuations grow into a stable pattern, then we must find a parameter space which ensures that $\mathcal{R}(\lambda) > 0$.

Substituting the expressions for $\tilde{n}$ and $\tilde{c}$ into equations (41) and (42) gives

$$\begin{pmatrix} \lambda\tilde{n} \\ \lambda\tilde{c} \end{pmatrix} = \begin{pmatrix} -k^2D - rN & k^2\chi N \\ 1/(1+N)^2 & -k^2 - 1 \end{pmatrix} \begin{pmatrix} \tilde{n} \\ \tilde{c} \end{pmatrix}, \tag{43}$$

which has solutions if and only if the following equation is satisfied:

$$\lambda^2 + [k^2(D+1) + 1 + rN]\lambda + h(k^2) = 0, \tag{44}$$

where

$$h(k^2) = Dk^4 + \left[rN + D - \frac{\chi N}{(1+N)^2}\right]k^2 + rN. \tag{45}$$

Perturbations to the steady states will grow if $\mathcal{R}(\lambda) > 0$ for some $k^2 > 0$. Considering the case $\lambda = 0$ we see that this occurs if $h(k^2) = 0$ has a real, non-negative root. This condition holds if

$$rN + D < \frac{N\chi}{(1+N)^2} \quad \text{and} \quad \left[rN + D - \frac{N\chi}{(1+N)^2}\right] > 4rND. \tag{46}$$

The wavenumbers of the admissible modes, *i.e.* the values of k which will give a spatially heterogeneous solution, are those such that $k_-^2 < k^2 < k_+^2$ where

$$k_\pm^2 = \frac{1}{2D}\left\{\left[\frac{N\chi}{(1+N)^2} - rN - D\right]^2 \pm \sqrt{\left[\frac{N\chi}{(1+N)^2} - rN - D\right]^2 - 4rND}\right\}. \tag{47}$$

The general solution of the linearised sytem (in 1D) can be written in the form

$$\tilde{n}(x,t) = e^{\lambda(k^2)t}\left[A\cos(kx) + B\sin(kx)\right], \tag{48}$$

$$\tilde{c}(x,t) = e^{\lambda(k^2)t}\left[\tilde{A}\cos(kx) + \tilde{B}\sin(kx)\right]. \tag{49}$$

The boundary condition at $x = 0$ gives $B, \tilde{B} = 0$ whilst the boundary condition at $x = L$ requires that for a non-trivial solution $kL = n\pi$ for $n = 0, 1, 2, \ldots$ The general solution can now be written as a combination of the admissible modes:

$$\tilde{n}(x,t) = \sum_n A_n e^{\lambda(k^2)t}\cos\left(\frac{n\pi x}{L}\right) \quad \text{and} \quad \tilde{c}(x,t) = \sum_n \tilde{A}_n e^{\lambda(k^2)t}\cos\left(\frac{n\pi x}{L}\right), \tag{50}$$

where the n satisfy

$$k_-^2 < \left(\frac{n\pi x}{L}\right)^2 < k_+^2. \tag{51}$$

Figure 6 (main text) shows the results of numerical solution of the model in one spatial dimension using the MATLAB function pdepe. The field is initially close to the homogeneous steady state, with small random fluctuations added to u throughout the domain. Over time, the fluctuations are amplified into a series of peaks and troughs in chemical concentration, with mode $n = 16$ chosen in this particular simulation: this is consistent with the set of admissible modes given in Figure 3. Parameters are as follows: $D = 0.25$, $\chi = 1.9$, $r = 0.01$ and $N = 1.0$. By way of illustration of the range of patterning possibilities, Figure 7 (main text) shows the results of numerical simulation of the model in two spatial dimensions, carried out using COMSOL MULTIPHYSICS.

We note that a specific mode, k_i^2, may be isolated by choosing the parameters such that $\lambda(k_i^2) = 0$ (Maini et al., 1991). In this case

$$rN + D - \frac{n\chi}{(1+N)^2} = -2\sqrt{rND} \quad \Rightarrow \quad k_i^2 = \sqrt{rN}D. \tag{52}$$

Figure 8 (main text) shows the results of numerical solution of the model in one spatial dimension using the MATLAB function pdepe with the initial disturbance localised to $x = 0$. We observe propagating patterning across the field, from left to right. The pattern corresponds to $n = 16$ which is consistent with the set of admissible modes given in Figure 3. Parameters are as follows: $D = 0.25$, $\chi = 1.9$, $r = 0.01$ and $N = 1.0$.

APPENDIX D. MECHANO-CHEMICAL MODEL

We consider cell density, $n(\boldsymbol{x}, t)$, ECM density, $\rho(\boldsymbol{x}, t)$, and the displacement vector of the ECM, $\boldsymbol{u}(\boldsymbol{x}, t)$, so that a material point in the matrix initially at $\boldsymbol{x}$ undergoes displacement to $\boldsymbol{x} + \boldsymbol{u}$. A more detailed description of the models can be found in (Murray et al., 1983; Oster et al., 1983; Maini, 1985; Murray and Maini, 1986; Perelson et al., 1986; Murray et al., 1988).

Cell density equation. The basic format for the cell density equation is a balance equation:

$$\frac{\partial n}{\partial t} = -\nabla.\boldsymbol{J} + M, \tag{53}$$

so that the rate of change in cell density is dependent on the cell flux $(\boldsymbol{J})$ and the proliferation rate (M). A simple assumption for M is that cell proliferation obeys a logistic equation: $M = rn(1-n)$, $r > 0$. The flux term includes terms describing cell motion, and these will be outlined below.

Convection. Cells may be passively transported due to deformations in the ECM:

$$\boldsymbol{J_c} = n\frac{\partial \boldsymbol{u}}{\partial t}, \tag{54}$$

where $\partial \boldsymbol{u}/\partial t$ is the velocity of ECM deformation.

Diffusion. Cells tend to undergo random diffusion in a homogeneous, isotropic medium – with movement down local density gradients. Cells may also sense densities further afield since they extend long filopodia, and in this case it is also relevant to include a non-local diffusive effect:

$$\boldsymbol{J_d} = -D_1 \nabla n + D_2 \nabla(\nabla^2 n), \tag{55}$$

where $D_1 > 0$ is the local diffusion coefficient and $D_2 > 0$ the non-local diffusion coefficient.
Haptotaxis. The traction effects of cells upon the matrix lead to gradients in ECM density. It is assumed that gradients in ECM density correspond to gradients in adhesive sites. Cells move up adhesive gradients as they may anchor more strongly to the ECM. This leads to a net flux of cells up the ECM gradient:

$$\boldsymbol{J_h} = n\nabla(a_1\rho - a_2\nabla^2\rho), \tag{56}$$

where $a_1 > 0$ represents the strength of the local contribution and $a_2 > 0$ the non-local contribution.

Taking the above factors into account, the cell density equation becomes

$$\begin{aligned} \frac{\partial n}{\partial t} &= -\nabla.\left(n\frac{\partial \boldsymbol{u}}{\partial t}\right) + \nabla.\left[D_1\nabla n - D_2\nabla(\nabla^2 n)\right] \\ &\quad -\nabla.\left[n\nabla(a_1\rho - a_2\nabla^2\rho)\right] + rn(1-n). \end{aligned} \tag{57}$$

Chemotaxis terms (motion up chemical gradients) and galvanotaxis terms (motion up gradients in electric potentials) may also be included if necessary.

Cell-matrix mechanical interaction equation. It is assumed that mechanical deformations are small and so the composite material of cells and ECM is modelled as a linear, isotropic viscoelastic continuum with stress tensor $\boldsymbol{\sigma}(\boldsymbol{x}, t)$. The time scale of embryonic development is very long compared to the spatial scale, which is very small: hence one may ignore inertial terms (since the Reynolds number is very small) and suppose that the traction forces generated by cells are in equilibrium with the viscoelastic restoring forces of the matrix and any other forces which act on the system. In this case the force balance equation becomes

$$\nabla.\boldsymbol{\sigma} + \rho\boldsymbol{F} = 0, \tag{58}$$

where $\boldsymbol{F}$ represents the external forces.
Stress tensor. Contributions from the ECM and cells give

$$\boldsymbol{\sigma} = \boldsymbol{\sigma_{ECM}} + \boldsymbol{\sigma_{cell}}. \tag{59}$$

The stress-strain relationship can be written using the usual expression for linear viscoelastic material as a sum of the viscous and elastic components (Landau and Lifshits, 2004):

$$\boldsymbol{\sigma_{ECM}} = \left[\mu_1\frac{\partial \boldsymbol{\varepsilon}}{\partial t} + \mu_2\frac{\partial \theta}{\partial t}\boldsymbol{I}\right] + E'\left[\boldsymbol{\varepsilon} + \nu'\theta\boldsymbol{I}\right], \tag{60}$$

where

$$E' = \frac{E}{1+\nu} \quad \text{and} \quad \nu' = \frac{\nu}{1-2\nu}. \tag{61}$$

In the above equations $\boldsymbol{I}$ is the unit tensor, μ_1, $\mu_2 > 0$ are the shear and bulk velocities of the ECM and $\boldsymbol{\varepsilon}$ and θ are the strain tensor and dilation, respectively, defined as

$$\boldsymbol{\varepsilon} = \frac{1}{2}\left(\nabla\boldsymbol{u} + \nabla\boldsymbol{u}^\top\right) \quad \text{and} \quad \theta = \nabla.\boldsymbol{u}, \tag{62}$$

where $E > 0$ is the Young's modulus and $\nu > 0$ the Poisson ratio.

The contribution to the stress tensor from the cells themselves comes from the traction forces. Experimental evidence suggests traction force increases with cell density, until cell-cell contact inhibition begins to play a role and the traction force decreases:

$$\tau(n) = \frac{\tau n}{1+\lambda n^2}. \tag{63}$$

$\tau \geq 0$ is a measure of the traction force generated by a cell and $\lambda > 0$. Assuming that non-local effects (similar to those for diffusion and haptotaxis) also play a role:

$$\boldsymbol{\sigma_{cell}} = \frac{\tau n}{1+\lambda n^2}\left[\rho + \gamma\nabla^2\rho\right], \tag{64}$$

where $\gamma > 0$ indicates the strength of the non-local contribution.

The body force can be derived by supposing that the matrix material is tethered to the underlying tissue, with body forces per unit ECM area proportional to the displacement of the ECM:

$$\boldsymbol{F} = -s\boldsymbol{u}, \tag{65}$$

where $s > 0$ characterises the strength of the elastic attachments.

Putting the above contributions back into the force balance equation gives

$$\nabla.\left[\mu_1\frac{\partial\boldsymbol{\varepsilon}}{\partial t} + \mu_2\frac{\partial\theta}{\partial t}\boldsymbol{I} + E'\left(\boldsymbol{\varepsilon} + \nu'\theta\boldsymbol{I}\right) + \nabla.\left\{\frac{\tau n}{1+\lambda n^2}\left(\rho + \gamma\nabla^2\rho\right)\right\}\right] - s\rho\boldsymbol{u} = 0. \tag{66}$$

Matrix conservation equation. The conservation equation can be written

$$\frac{\partial\rho}{\partial t} + \nabla.\left(\rho\frac{\partial\boldsymbol{u}}{\partial t}\right) = 0, \tag{67}$$

that is, matrix movements are solely due to convective effects.

Simplified model. In order to present some simplified analysis, we make the following assumptions: (i) cells cannot diffuse $\Rightarrow D_1 = 0 = D_2$; (ii) cells cannot sense adhesive gradients $\Rightarrow a_1 = 0 = a_2$; (iii) there is no cell proliferation or death $\Rightarrow r = 0$. In this case, cells are simply convected by the ECM, which is thought to be one of the major transport processes (Murray, 2003).

In one spatial dimension, the equations become

$$0 = \frac{\partial n}{\partial t} + \frac{\partial}{\partial x}\left(n\frac{\partial u}{\partial t}\right), \tag{68}$$

$$0 = \frac{\partial}{\partial x}\left[\mu\frac{\partial^2 u}{\partial x\partial t} + \frac{\partial u}{\partial x} + \frac{\tau' n}{1+\lambda n^2}\left(\rho + \gamma\frac{\partial^2\rho}{\partial x^2}\right)\right] - s'\rho u, \tag{69}$$

$$0 = \frac{\partial\rho}{\partial t} + \frac{\partial}{\partial x}\left(\rho\frac{\partial u}{\partial t}\right), \tag{70}$$

where

$$\mu = \frac{\mu_1+\mu_2}{E'(1+\nu')}, \quad \tau' = \frac{\tau}{E'(1+\nu')} \quad \text{and} \quad s' = \frac{s}{E'(1+\nu')}. \tag{71}$$

The spatially uniform steady state in which we will be interested is $(n_0, \rho_0, u_0) = (1, 1, 0)$. Linearising about the steady state by writing $n = n_0 + \tilde{n}$, $\rho = \rho_0 + \tilde{\rho}$ and $u = u_0 + \tilde{u}$, where $\tilde{n}$, $\tilde{\rho}$, $\tilde{u}$

are small, we have, to first order,

$$0 = \frac{\partial \tilde{n}}{\partial t} + \frac{\partial^2 \tilde{u}}{\partial x \partial t}, \tag{72}$$

$$0 = \frac{\partial}{\partial x}\left[\mu \frac{\partial^2 \tilde{u}}{\partial x \partial t} + \frac{\partial \tilde{u}}{\partial x} + \tau_1 \tilde{n} + \tau_2 \left(\tilde{\rho} + \gamma \frac{\partial^2 \tilde{\rho}}{\partial x^2}\right)\right] - s' \tilde{u}, \tag{73}$$

$$0 = \frac{\partial \tilde{\rho}}{\partial t} + \frac{\partial^2 \tilde{u}}{\partial x \partial t}, \tag{74}$$

where

$$\tau_1 = \frac{\tau'(1-\lambda)}{(1+\lambda)^2} \quad \text{and} \quad \tau_2 = \frac{\tau'}{1+\lambda}. \tag{75}$$

Once again, we consider finding solutions of the form $\tilde{n} = \alpha \exp(\lambda t + ikx)$, $\tilde{\rho} = \beta \exp(\lambda t + ikx)$ and $\tilde{u} = \delta \exp(\lambda t + ikx)$. Substituting into equations (72)-(74) gives

$$\begin{pmatrix} \lambda\tilde{n} \\ \lambda\tilde{\rho} \\ \lambda\tilde{u} \end{pmatrix} = \begin{pmatrix} \lambda & 0 & ik\lambda \\ ik\tau_1 & (ik - ik^3\gamma)\tau_2 & -k^2(\mu\lambda + 1) - s' \\ 0 & \lambda & ik\lambda \end{pmatrix} \begin{pmatrix} \tilde{n} \\ \tilde{\rho} \\ \tilde{u} \end{pmatrix}, \tag{76}$$

which has solutions if and only if

$$\lambda^2 \left[k^2 \mu \lambda + b(k^2)\right] = 0, \tag{77}$$

where

$$b(k^2) = \gamma \tau_2 k^4 + (1 - \tau_1 - \tau_2)k^2 + s'. \tag{78}$$

Hence $\lambda(k^2) > 0$ for some $k^2 \neq 0$, and spatially heterogeneous solutions exist, if and only if $b(k^2) < 0$. This gives the first condition: $\tau_1 + \tau_2 > 1$. The minimum of $b(k^2)$ occurs at

$$k^2_{min} = \frac{\tau_1 + \tau_2 - 1}{2\tau_2\gamma} \quad \Rightarrow \quad b(k^2_{min}) = s' - \frac{(\tau_1 + \tau_2 - 1)^2}{4\tau_2\gamma}. \tag{79}$$

Substituting the expressions for τ_1 and τ_2 into the above gives the second condition for spatially heterogeneous solutions:

$$\tau'^2 - \tau'(1+\lambda)^2\left[1 + \gamma s'(1+\lambda)\right] + \frac{(1+\lambda)^4}{4} > 0. \tag{80}$$

In this way, we may treat τ', the parameter measuring traction strength, as a bifurcation parameter and show that the surface

$$\tau'_c(\lambda, s', \gamma) = (1+\lambda^2)\left[1 + s'\gamma(1+\lambda)\right]\left\{1 + \sqrt{1 - \frac{1}{[1 + s'\gamma(1+\lambda)]}}\right\}, \tag{81}$$

defines the boundary between spatially homogeneous solutions, $\tau' < \tau'_c$, and spatially heterogeneous solutions, $\tau' > \tau'_c$.

Assuming zero flux boundary conditions for n and ρ and that $u(x,t) = 0$ for $x = 0, L$, the general solution can be written as a sum of the admissible modes:

$$\tilde{n}(x,t) = \sum_n A_n e^{\lambda(k^2)t} \cos\left(\frac{n\pi x}{L}\right), \tag{82}$$

$$\tilde{\rho}(x,t) = \sum_n \tilde{A}_n e^{\lambda(k^2)t} \cos\left(\frac{n\pi x}{L}\right), \tag{83}$$

$$\tilde{u}(x,t) = \sum_n \breve{A}_n e^{\lambda(k^2)t} \sin\left(\frac{n\pi x}{L}\right), \tag{84}$$

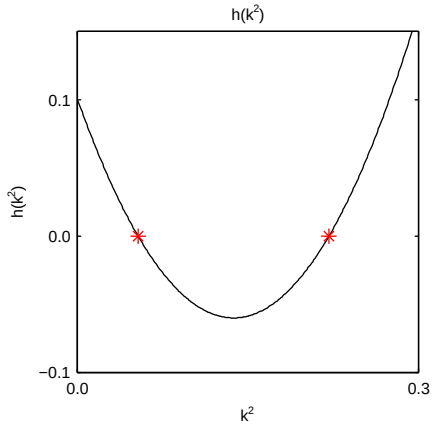

Figure 4. A plot of $b(k^2)$ given by equation (78). The roots are given approximately by $k_-^2 = 0.0531$ and $k_+^2 = 0.2214$ (red asterisks), which gives a range of possible modes of $n = 6, 7, \ldots, 11$. Parameters are as follows: $\mu = 0.1$, $\tau' = 15.0$, $\lambda = 2.0$, $\gamma = 1.7$ and $s' = 0.1$.

where the n satisfy

$$k_-^2 < \left(\frac{n\pi x}{L}\right)^2 < k_+^2 \quad \text{and} \quad k_\pm^2 = \frac{(\tau_1 + \tau_2 - 1) \pm \sqrt{(\tau_1 + \tau_2 - 1) - 4\gamma\tau_2 s'}}{2\gamma\tau_2}. \tag{85}$$

Numerical results. A detailed numerical study of the original model was carried out by Perelson and co-workers in (Perelson et al., 1986). They carry out a full investigation of the pattern forming capabilities of the system and develop a technique for non-linear mode selection. Finally they apply their method to sequential feather bud formation in the chick embryo.

REFERENCES

R. E. Baker. *Periodic pattern formation in developmental biology: a study of the mechanisms underlying somitogenesis*. PhD thesis, University of Oxford, 2005.

R. E. Baker, S. Schnell, and P. K. Maini. Formation of vertebral precursors: past models and future predictions. *J. Theor. Med.*, 5:23–35, 2003.

R. E. Baker, S. Schnell, and P. K. Maini. A clock and wavefront mechanism for somite formation. *Dev. Biol.*, 293:116–126, 2006a.

R. E. Baker, S. Schnell, and P. K. Maini. A mathematical investigation of a clock and wavefront model for somitogenesis. *J. Math. Biol.*, 52:458–482, 2006b.

J. R. Collier, D. McInerney, S. Schnell, P. K. Maini, D. J. Gavaghan, P. Houston, and C. D. Stern. A cell cycle model for somitogenesis: mathematical formulation and numerical solution. *J. Theor. Biol.*, 207:305–316, 2000.

J. Dubrulle and O. Pourquie. From head to tail: links between the segmentation clock and antero-posterior patterning of the embryo. *Curr. Op. Genet. Dev.*, 12:519–523, 2002.

J. Dubrulle, M. J. McGrew, and O. Pourquie. Fgf signalling controls somite boundary position and regulates segmentation clock control of spatiotemporal hox gene activation. *Cell*, 106:219–232, 2001.

A. Gierer and H. Meinhardt. A theory of biological pattern formation. *Kybernetik*, 12:30–39, 1972.

L. D. Landau and E. M. Lifshits. *Theory of Elasticity*, volume 7 of *Course of Theoretical Physics*. Butterworth-Heinemann Ltd, 3rd edition, 2004.

P. K. Maini. *On mechano-chemical models for morphogenetic pattern formation*. PhD thesis, University of Oxford, 1985.

P. K. Maini, M. R. Myerscough, K. H. Winters, and J. D. Murray. Bifurcating spatially heterogeneous solutions in a chemotaxis model for biological pattern generation. *Bull. Math. Biol.*, 53: 701–719, 1991.

D. McInerney, S. Schnell, R. E. Baker, and P. K. Maini. A mathematical formulation for the cell cycle model in somitogenesis: parameter constraints and numerical solutions. *IMA J. Math. Appl. Med. & Biol.*, 21:85–113, 2004.

J. D. Murray. *Mathematical Biology II: Spatial Models and Biochemical Applications*, volume II. Springer-Verlag, 3rd edition, 2003.

J. D. Murray and P. K. Maini. A new approach to the generation of pattern and form in embryology. *Sci. Prog. Oxf.*, 70:539–553, 1986.

J. D. Murray, G. F. Oster, and A. K. Harris. A mechanical model for mesenchymal morphogenesis. *J. Math. Biol.*, 17:125–129, 1983.

J. D. Murray, P. K. Maini, and R. T. Tranquillo. Mechanochemical models for generating biological pattern and form in development. *Phys. Rep.*, 171:59–84, 1988.

M. R. Myerscough, P. K. Maini, J. D. Murray, and K. H. Winters. *Two dimensional pattern formation in a chemotactic system*, pages 65–83. Dynamics of Complex Interconnected Biological Systems. Birkhauser, Boston, 1990.

M. R. Myerscough, P. K. Maini, and K. J. Painter. Pattern formation in a generalised chemotactic model. *Bull. Math. Biol.*, 60:1–26, 1998.

G. F Oster, J. D. Murray, and A. K. Harris. Mechanical aspects of mesenchymcal morphogenesis. *J. Embryol. Exp. Morphol.*, 78:83–125, 1983.

A. S. Perelson, P. K. Maini, J. D. Murray, J. M. Hyman, and G. F. Oster. Nonlinear pattern selection in a mechanical model for morphogenesis. *J. Math. Biol.*, 24:525–541, 1986.

D. R. N. Primmett, W. E. Norris, G. J. Carlson, R. J. Keynes, and C. D. Stern. Periodic anomalies induced by heat shock in the chick embryo are associated with the cell cycle. *Development*, 105:119–130, 1989.

J. Schnakenberg. Simple chemical reaction systems with limit cycle behaviour. *J. Theor. Biol.*, 81:389–400, 1979.

S. Schnell, P. K. Maini, D. McInerney, D. J. Gavaghan, and P. Houston. Models for pattern formation in somitogenesis: a marriage of cellular and molecular biology. *C. R. Biologies*, 325: 179–189, 2002.

C. J. Tabin and R. L. Johnson. Developmental biology: clocks and hox. *Nature*, 412:780–781, 2001.

A. M. Turing. The chemical basis of morphogenesis. *Roy. Soc. Lond. Phil. Trans. B*, 237:37–72, 1952.